JOURNAL OF GEOPHYSICAL RESEARCH, VOL. 101, NO. D3, PAGES 6795–6802, MARCH 20, 1996

Interaction of peroxynitric acid with solid H_2O ice

Zhuangjie Li,[1] Randall R. Friedl, Steven B. Moore, and Stanley P. Sander
Jet Propulsion Laboratory, California Institute of Technology, Pasadena

Abstract. The uptake of peroxynitric acid (PNA), HO_2NO_2 or HNO_4, on solid H_2O ice at 193 K (−80°C) was studied using a fast flow-mass spectrometric technique. An uptake coefficient of 0.15 ± 0.10 was measured, where the quoted uncertainty denotes 2 standard deviations. The uptake process did not result in the production of gas phase products. The composition of the condensed phase was investigated using programmed heating (3 K min^{-1}) of the substrate coupled with mass spectrometric detection of desorbed species. Significant quantities of HNO_4 and HNO_3 desorbed from the substrates at temperatures above 225 K and 246 K, respectively. The desorbed HNO_3, which was less than 9% of the desorbed HNO_4 and remained unchanged upon incubation of the substrate, was likely due to impurities in the HNO_4 samples rather than reaction of HNO_4 on the substrate. The onset temperatures for HNO_4 desorption increased with increasing H_2O to HNO_4 ratios, indicating that HNO_4, like HNO_3, tends to be hydrated in the presence of water. These observations suggest possible mechanisms for removal of HNO_4 or repartitioning of total odd nitrogen species in the Earth's upper troposphere and stratosphere.

Introduction

Atmospheric NO_x($NO + NO_2$) and HO_x ($OH + HO_2$) species are coupled together by two reactions resulting in acid formation [*Niki et al.*, 1977; *Howard*, 1977; *Anderson et al.*, 1974], namely,

(R1) $HO_2 + NO_2 + M \rightarrow HOONO_2 + M$

(R2) $OH + NO_2 + M \rightarrow HONO_2 + M$

The important role of nitric acid, HNO_3, as a relatively stable reservoir of atmospheric NO_x has long been recognized from global gas phase model calculations and field observations [*Hudson and Reed*, 1979]. Recent laboratory and field studies have also identified HNO_3 as a key species in denitrification of the wintertime polar stratosphere through gas-to-particle conversion followed by particle subsidence [*Molina et al.*, 1987; *Fahey et al.*, 1990; *Considine et al.*, 1992; *Kondo et al.*, 1994].

Peroxynitric acid, HNO_4, has received considerably less attention due to its relatively low atmospheric abundance. Although atmospheric production rates of HNO_4 are approximately equal to those of HNO_3 in the lower stratosphere and upper troposphere (e.g., at 25 km $P(HNO_4)/P(HNO_3) = k_1/k_2 \times [HO_2]/[OH] \approx 0.1 \times 7 = 0.7$) [*DeMore et al.*, 1994], ambient concentrations of HNO_4 (~0.2 parts per billion by volume (ppbv)) are significantly less than HNO_3 (~6.5 ppbv) (G. T. Toon, M. R. Gunson, and R. J. Salawitch, private communication, 1995) due to relatively rapid photolysis of HNO_4 and reaction of HNO_4 with OH.

(R3) $HNO_4 + h\nu \rightarrow$ products

(R4) $OH + HNO_4 \rightarrow$ products

On the basis of existing kinetics data the lower stratospheric lifetime of HNO_4 with respect to these processes ranges from approximately several days in the summer tropics to several weeks over the springtime pole [*Graham et al.*, 1977, 1978a]. Since both processes involving HNO_4 likely regenerate HO_2 and NO_2 in the atmosphere, the role of HNO_4 relative to HNO_3 is presumably that of a short- or medium-term NO_x reservoir.

Heterogeneous processing of stratospheric HNO_4 carries the potential to substantially alter the role of HNO_4 in NO_y chemistry. Since HNO_4 can be viewed as an inorganic peracid, a mixed hydride of two acids, or as a peroxynitrite, it may participate in free radical and/or ionic reactions, the latter type having been postulated to explain the heterogeneous reaction of HCl with $ClONO_2$, a reaction that is largely responsible for formation of active chlorine in the polar stratosphere [*Molina et al.*, 1987]. In the case of HNO_4, heterogeneous chemical pathways of interest are those that result in a significant shift in the NO_y partitioning toward either more active NO_y species (i.e., NO, NO_2, or HONO) or the less active NO_y species such as HNO_3. Previous investigations have provided some evidence for the former pathway. In particular, *Zhu et al.* [1993] have obtained evidence for formation of HONO from the decomposition of HNO_4 on glass at 298 K. *Logager and Sehested* [1993] have proposed that decomposition of peroxynitric acid (PNA) in solution is initiated by unimolecular decomposition to yield HONO. Since HONO is readily photolyzed in the stratosphere to yield NO [*Cox*, 1974], heterogeneous chemistry may facilitate the destruction of reservoir HNO_4 and the reformation of NO_x.

The potential atmospheric impact of HNO_4 heterogeneous chemistry can be constrained by consideration of the frequency of collision (z) between HNO_4 and the background aerosol surface,

$$z = (c/4)A \quad (1)$$

where c is the average HNO_4 velocity and A is the area density of stratospheric aerosol. At 20-km altitude, where a typical value of A is 6×10^{-9} cm^2 cm^{-3} [*Turco et al.*, 1982; *Deshler et*

[1]Now at Department of Atmospheric Sciences, University of Illinois at Urbana-Champaign.

Paper number 96JD00065.
0148-0227/96/96JD-00065$05.00

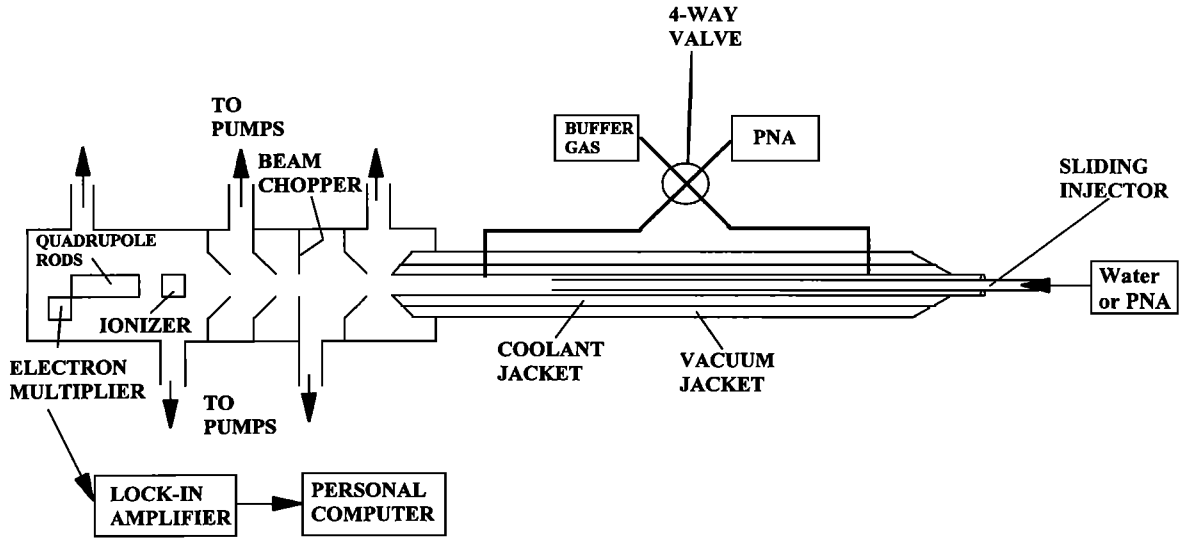

Figure 1. Experimental setup for studying reaction of peroxynitric acid (PNA) with water at low temperature.

al., 1992] and c is approximately 2×10^4 cm s^{-1}, the collision frequency is 3×10^{-5} s^{-1}. Since the loss rate of HNO_4 is equal to the product of the collision frequency and the fraction of collisions (γ) resulting in reaction, the value for γ must be greater than 0.03 for heterogeneous loss rates to be competitive with photolysis and reaction with OH.

In the present study we have obtained data on the interaction of HNO_4 with solid H_2O ice and HCl-doped H_2O ice. Experimental results were obtained using both a traditional, steady state flow tube technique and a fast switch variant of the flow tube technique. The latter technique was used to check for surface saturation by HNO_4. In this paper we report results from both experimental approaches and derive surface probabilities for HNO_4 on solid H_2O ice and HCl-doped H_2O ice at 190 K.

Experimental

The experimental apparatus and its application to gas-solid interactions are illustrated in Figure 1. In brief the apparatus consisted of a conventional fast flow reactor that was modified for heterogeneous studies at low temperature and a mass spectrometer connected to the downstream end of the reactor. A 40-cm-long, 2.54-cm OD Pyrex tube served as the main reactor. PNA was admitted into the reactor through one of three ports, namely, a 120-cm-long, 0.63-cm OD moveable injector that was heated with nitrogen gas at room temperature and coaxial with the reactor tube or one of a set of entrance ports located within the cooled portion of the reactor but outside of the ice-coated region. A four-way valve connected to each of the latter set of ports by 3.2-mm-diameter polytetrafluoroethylene (PTFE) tubing allowed the PNA flow direction to be rapidly switched between the downstream and upstream ports. The time delay in PNA arrival at the detector caused by switching the four-way valve was estimated to be less than 50 ms, based on a sample flow velocity of ~2800 cm s^{-1} and a maximum traveling distance of 140 cm after alteration of the flow direction.

Total pressure in the reactor was measured by a 1-torr MKS baratron with accuracy of ±0.001 torr. Most mass spectrometer calibrations and experiments were carried out under total pressure of 0.5 torr, while a few trials were run at total pressure of 1 torr in the reactor. The reactor temperature was controlled by circulation of cooled methanol through an outer Pyrex jacket and measured by a pair of thermocouples located at the downstream and upstream ends. For the current experiments, temperatures were maintained at 184 ~ 193 K with an overall measurement accuracy of ±1 K. The methanol circulator was equipped with a heater that served to either stabilize the temperature to within ±0.5 K or warm up the reactor at a rate of about 3 K min^{-1}.

Ice films were prepared by bubbling helium carrier gas through a liquid water trap and passing the saturated gas flow into the reactor through the sliding injector. Film deposition was initiated with the injector tip at the downstream edge of the cold jacket and proceeded by withdrawal of the injector in 1-cm increments. The thickness of the ice film was controlled by varying the deposition time between each injector movement. Deposition times were varied between 10 s and 2 min, resulting in film thicknesses between 13 and 160 μm, respectively. Calculation of film thickness was accomplished by consideration of the geometric surface area of the reactor wall (8 cm^2 cm^{-1}), the amount of deposited water, and the bulk density of vapor-deposited water ice (i.e., 0.63 g cm^{-3} [*Keyser and Leu*, 1993]). The amount of ice was calculated from the water vapor pressure at 293 K, the mass flow rate of the helium-water mixture, and the total deposit time. Some of the deposited ice samples were collected in a U tube at 77 K and weighed on an analytical balance. It was found that the calculated amount of water agreed with that measured within 5%.

HNO_4 was synthesized by slowly adding ~1 g NO_2BF_4 (Aldrich) into ~5 mL of cold (≈0°C) 90% H_2O_2 [*Kenley et al.*, 1981]. The solution containing the HNO_4 was transferred to a glass bubbler for use in the experiments. The bubbler was maintained at 273 K and was connected to the flow reactor via 0.25-inch OD Teflon tubing. A cold trap (~258 K) was inserted between the HNO_4 sample bubbler and the reactor in order to reduce the amount of H_2O_2 impurity in the gas flow. HNO_4 sample flows were established by passage of helium through the bubbler.

The purities of several HNO_4 samples were checked by filling a small absorption cell and subjecting it to Fourier transform infrared analysis [*Graham et al.*, 1978a, b; *May and Friedl*,

Table 1. Mass Spectral Intensities for Peroxynitric Acid (PNA), NO_2, H_2O_2, HNO_3, and H_2O

	Ion					
	H_2O^+	NO^+	HO_2^+	$H_2O_2^+$	NO_2^+	HNO_3^+
m/e	18	30	33	34	46	63
PNA		25	6		180	
NO_2		49			55	
H_2O_2			2	58		
HNO_3		9			93	3
H_2O	10					

Values are in mV per millitorr (except for the first row).

1993; *Molina and Molina*, 1981]. Infrared spectra were taken by a Bomem DA3+.002 Fourier transform spectrometer equipped with a liquid nitrogen-cooled Cu:Ge detector. Impurities in the HNO_4 solution were identified in the IR spectrum and ascribed to H_2O_2, HNO_3, NO_2, and H_2O. The relative amounts of the H_2O_2, HNO_3, and NO_2 impurities varied between HNO_4 samples but were always less than 20%; water concentrations were approximately 5 times greater than HNO_4 concentrations. Greater than tenfold reduction of HNO_3 and NO_2 impurities could be achieved by bubbling helium through the sample solution for ~20 min prior to experimental use of the sample. The 258 K cold trap was found to reduce the amount of H_2O_2 by approximately a factor of 5, although H_2O_2 remained along with H_2O, the major impurities entering the reactor.

The Extranuclear electron impact mass spectrometer system employed in this study consisted of an ionizer operated at 25 eV, a quadrupole mass filter, and a channeltron. Beam modulation was achieved with a 200-Hz tuning fork type chopper placed inside the second stage of the three-stage differentially pumped chamber. Ion beam signals from the channeltron were fed to a lock-in amplifier (Stanford Research Systems model 510) and stored on a personal computer following signal digitization with a computer-resident analog to digital converter (Analog Devices RTI/815).

HNO_4 was monitored at *m/e* ratios of 33, 46, and 30. Mass spectral intensities of HNO_4 as well as the impurity species and/or reaction products H_2O_2, NO_2, HNO_3, and H_2O are given in Table 1. Although all of the HNO_4 mass peaks are subject to spectral interference from the other important species, in practice, during decay measurements the signals at both $m/e = 33$ (HO_2^+) and $m/e = 46$ (NO_2^+) were essentially free from H_2O_2, HNO_3, and NO_2 interference on account of (1) the extremely low H_2O_2 and HNO_3 sublimation pressures at 193 K and (2) NO_2 being distilled out of the HNO_4 solution after sample bubblings. This fact was confirmed by checking for signals at the H_2O_2 and HNO_3 parent peaks at $m/e = 34$ ($H_2O_2^+$) and $m/e = 63$ (HNO_3^+). In most cases, no signal was detected at $m/e = 63$, thereby constraining the amount of signal at $m/e = 46$ that was due to HNO_3 to less than 2% of the total $m/e = 46$ signal. Possible interference from NO_2 at $m/e = 46$ was discounted by reference to $m/e = 30$ signal. Specifically, HNO_4 and NO_2 could be differentiated by their substantially different signal ratios (i.e., $[m/e = 46]/[m/e = 30] = 7$ for HNO_4 and 1.1 for NO_2). At the beginning of sample purification procedures the observed signal ratios could be as low as 5 (i.e., 20% NO_2 impurity), but after distillation the signal ratio corresponded to pure HNO_4 and remained so during the decay measurements. As both $m/e = 33$ and $m/e = 46$ can be predominately ascribed to HNO_4, we used $m/e = 46$ in most of our experiments since a factor of 30 higher sensitivity of $m/e = 46$ than $m/e = 33$ allowed much lower HNO_4 concentration detection using $m/e = 46$. The mass spectrum of HONO was not characterized for this experiment; however, we expect that its fragmentation pattern resembles that of NO_2 rather than HNO_4.

Approximate calibrations of the mass spectral signals were obtained for all of the species listed in Table 1. For the stable gases such as HNO_3, NO_2, and H_2O_2, dilute samples were prepared by combining He with vapor from pure HNO_3 and NO_2 or 90% H_2O_2 in H_2O. Absolute concentrations were obtained from measurements of total reactor pressures and gas flow rates (i.e., buffer gas and dilute sample flow rates). In the case of H_2O_2 the partial vapor pressure was determined by subtracting the water vapor contribution from the total pressure measured over the 90% H_2O_2 solution. For HNO_4, concentrations were determined from the flow rate of helium carrier gas and the fraction of HNO_4 in the flow. The HNO_4 partial pressure in the bubbler was derived from infrared absorbances of gaseous samples extracted from the bubbler using the HNO_4 cross sections reported by *Molina and Molina* [1981] and *Graham et al.* [1978b].

For most investigations of HNO_4 uptake on substrates, partial pressures of gaseous HNO_4 in the reactor were restricted to less than 0.1 mtorr. On the basis of data from *Kenley et al.* [1981] and *May and Friedl* [1993] we estimate that these amounts are significantly less than the equilibrium vapor pressure of HNO_4 at 193 K. Several measurements for HNO_4 uptake on ice were made with PNA partial pressure greater than 0.1 mtorr to examine the effect of PNA concentration on the sticking process.

Results

Fast Switch Transient Experiments

A qualitative appraisal of the interaction between HNO_4 and solid H_2O ice was accomplished by rapidly exposing the entire ice substrate to the gas flow and observing the transient signal behavior. Exposure of a surface to HNO_4 was initiated by switching the gas flow from an entry port located near the mass spectrometer inlet and downstream of the substrate to one located upstream of the substrate. The additional transit distance of the flow was responsible for a rapid initial decrease in observed signal followed by rapid recovery. The transit time was approximately 50 ms as determined from a switched flow experiment through an uncoated, room temperature reactor.

Typical HNO_4 temporal profiles are shown in Figures 2 and 3 for cold-uncoated and cold-coated reactors, respectively. In the cold-uncoated reactor case, signal recovery was characterized by two rates: a fast rate (1%/ms) similar to that observed in the room temperature reactor but prematurely ending at only 80% signal recovery and a slow subsequent rate (<0.25%/min) extrapolating to signal recovery on timescales greater than 1 hour. Although the signal behavior clearly indicates the occurrence of HNO_4 uptake on the reactor walls, no gas phase signals attributable to likely reaction products were detected. On the basis of these observations alone it is unclear whether the observed uptake phenomenology is attributable to HNO_4 condensation, where the inferred sublimation pressure would equal a value 0.8 times the initial HNO_4 vapor pressure (≈0.1 mtorr), or to interaction of HNO_4 with condensed impurities present in the HNO_4 such as H_2O and H_2O_2. On the basis of

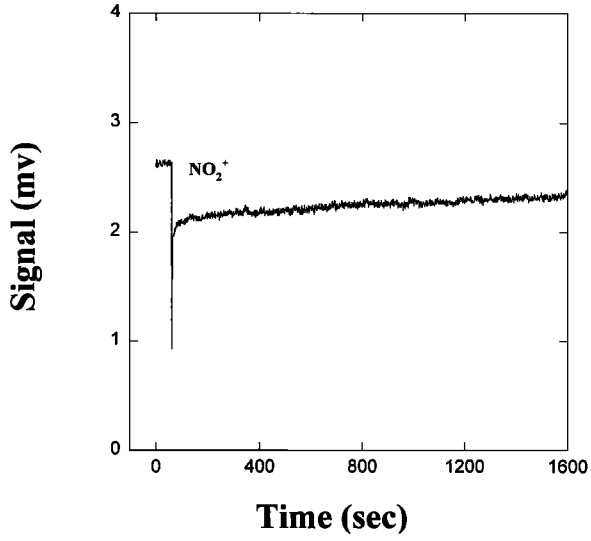

Figure 2. NO_2^+ signal (predominately due to HNO_4) as function of time when flowing PNA through Pyrex reactor surface at 190 K. The initial concentration of PNA was 1.5×10^{-5} torr.

our measurements of the impurity levels in the HNO_4 samples, the thicknesses of films resulting from deposition of the impurities over the course of the observations were of the order of 0.1 μm. Amounts of deposited HNO_4 were roughly a factor of 5 less than the H_2O impurity deposits.

A dramatically enhanced uptake of HNO_4 was observed in the ice-coated reactor case, providing strong evidence for the occurrence of a substantial interaction between the H_2O ice and HNO_4. Saturation of the surface, as indicated by signal recovery, occurred at a relatively slow rate of approximately 4%/min for the first 20 min, leveling off to a rate of less than 0.25%/min thereafter. The continuation of HNO_4 uptake after 20 min is similar to the behavior observed in the uncoated case and, in light of profound uptake at early times, is most likely attributed to additional HNO_4 uptake on fresh deposits of H_2O impurities contained in the HNO_4 flow.

The amount of HNO_4 deposited during the first 20 min is of the order of 10^{19} molecule, far exceeding monolayer coverage ($\theta > 1$) of the 20-cm-long ice-covered surface (θ was calculated assuming a monolayer of HNO_4 to be approximately 5×10^{14} molecule cm^{-2} [*Hanson*, 1992]). As in the uncoated case an exhaustive mass spectral search provided no evidence for production of gas phase species from the surface interaction. Possible alternative explanations for the large uptake include reactions to produce condensed phase species such as HNO_3, availability of internal ice surface area, or formation of HNO_4 hydrates or solid HNO_4/H_2O solutions. Additional information on these possibilities was obtained during the desorption experiments to be described in a later section of this report.

Movable Injector Experiments

As revealed by the results of the fast switch flow technique, the H_2O ice substrates adsorb significant quantities of HNO_4 but are eventually saturated with respect to further uptake. The slow rate of the saturation process allowed us to make precise measurements of the HNO_4 uptake kinetics (i.e., sticking probability) using the commonly employed movable injector technique. Kinetics data were obtained by passing HNO_4 through the movable injector and admitting the flow into the reactor at various points along the ice substrate. In a similar manner to the ice deposition procedure the experimental trials were started with the injector tip at the downstream end of the ice-coated region. The injector position was changed in 5-cm steps at approximately 1-min intervals to allow for signal averaging and data collection.

The method used for retrieving sticking coefficients from the collected data is well known [*Howard*, 1979]. For a significant first-order wall loss in a steady state tubular flow reactor the loss rate can be written simply as

$$d[HNO_4]/dt = \langle u \rangle d[HNO_4]/dz = -k[HNO_4] \quad (2)$$

where k is the first-order rate constant, t is the contact time between the reactor wall and the gas flow, and $[HNO_4]$ is the concentration of HNO_4 at time t. The contact time is calculated from the average carrier flow velocity, $\langle u \rangle$, and the distance traveled by the flow after exit from the movable injector. The rate constant can be determined from a regression of a plot of the logarithm of HNO_4 signal versus time.

Figure 4 represents a typical plot of the logarithm of PNA signal (m/e = 46 and 33) versus time. The observed logarithmic signal decays displayed good linearity over the time domain studied, and retrieved decay slopes were essentially identical for the m/e = 33 and m/e = 46 signal data. Data were corrected for radial and ice pore diffusion using the program developed by *Brown* [1978] and modified by *Keyser et al.* [1991]. The sticking coefficient γ (i.e., the fraction of surface collisions resulting in removal of HNO_4) is calculated from

$$\gamma = 2r_0 k_g/(\omega + r_0 k_g) \quad (3)$$

where r_0 is the radius of the reactor and ω the average molecular speed. We carried out a total of 23 runs on ice with the following range in parameters: film thicknesses between 13 and 160 μm, total reactor pressures between 0.5 and 1 torr, total flow rates between 500 and 1000 sccm, temperatures between

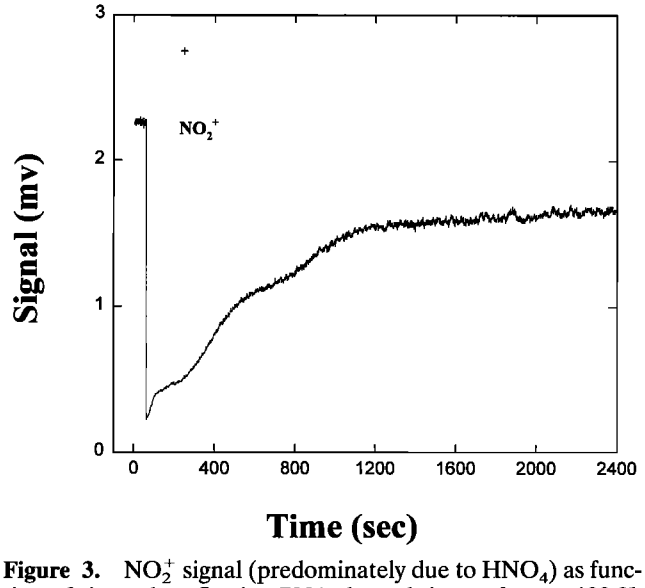

Figure 3. NO_2^+ signal (predominately due to HNO_4) as function of time when flowing PNA through ice surface at 190 K. The thickness and the length of the ice film were 13.4 μm and 20 cm, and the initial concentration of PNA was 1.2×10^{-5} torr.

183 and 193 K, and initial HNO_4 partial pressures between 0.012 and 0.45 mtorr.

The results for each experimental trial are listed in Table 2. Calculated sticking coefficients for HNO_4 on ice are independent of the experimental conditions related to ice thickness, temperature, and initial HNO_4 concentration. Combining all of the experimental data yields an average value for the sticking coefficient of 0.15 ± 0.10, where the reported uncertainty is at the 2σ limit.

As a slight extension of this study we briefly investigated the possibility of a heterogeneous reaction involving HNO_4 and HCl. We first doped HCl (~4×10^{20} molecules) on the ice surface and then introduced PNA to the ice surface with and without introducing HCl in the gas phase. No change in the measured uptake coefficient relative to the HNO_4/H_2O ice only case was observed, indicating the absence of a significant heterogeneous reaction between HNO_4 and HCl at low temperature. In support of this conclusion we were unable to detect any new gas phase chlorine-containing species such as HOCl or Cl_2.

Product Studies

As stated previously a methodical mass spectral search conducted in concert with HNO_4 uptake trials revealed no evidence for new gas phase species. The lack of gaseous product formation associated with the rapid, large-scale uptake of HNO_4 on H_2O ice points to the likelihood of physical or chemical adsorption of the HNO_4.

$$\text{(R5a)}\quad HO_2NO_{2(g)} + H_2O_{(s)} \rightarrow HO_2NO_{2(s)} + H_2O_{(s)}$$

$$\text{(R5b)}\quad HO_2NO_{2(g)} + H_2O_{(s)} \rightarrow HO_2NO_2 \cdot (H_2O)_{n(s)}$$

Another possibility is reaction of the HNO_4 to produce condensed or solvated species. An example of the latter process is given by (R5b) or (R5c), which involves HNO_3 production.

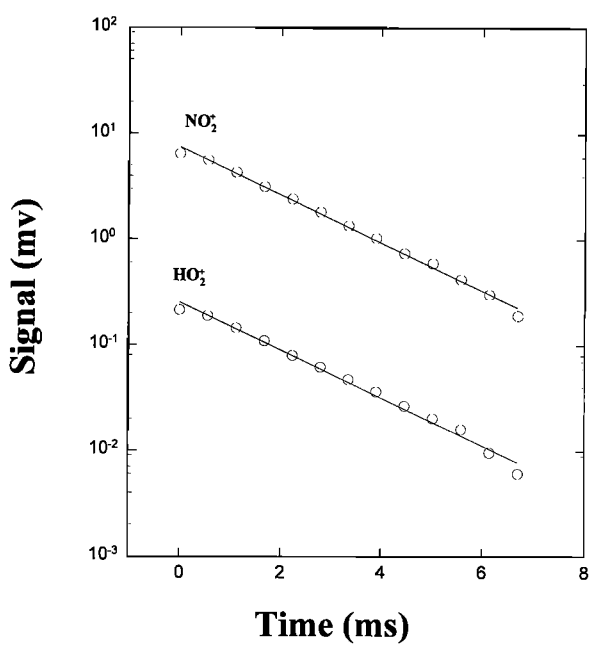

Figure 4. Typical HNO_4 (as inferred from both NO_2^+ and HO_2^+) decay on ice surface (160 μm thick) at 189 K. The experimental conditions for the plot were $P_{total} = 0.51$ torr, $P_{PNA} = 4.1 \times 10^{-5}$ torr, and $v_{flow} = 1800$ cm s^{-1}.

Table 2. Sticking Probability for Peroxynitric Acid on Ice Surfaces

h,* μm	P_{total}, torr	F_{total}, sccm	Temperature, K	[PNA], mtorr	k_{obs}, s^{-1}	k_g, s^{-1}	γ
13.5	0.92	997	192	0.038	364	1678	0.17
13.4	0.91	957	189	0.068	288	751	0.081
13.6	0.93	985	187	0.45	332	1363	0.14
13.9	0.50	530	193	0.063	349	580	0.063
13.7	0.50	533	193	0.060	436	881	0.090
13.5	0.50	536	193	0.33	510	1264	0.13
13.6	0.50	527	193	0.024	458	975	0.10
13.5	0.50	524	193	0.031	577	1824	0.19
13.5	0.50	523	189	0.056	566	1700	0.17
13.5	0.50	525	191	0.082	554	1598	0.16
81.5	0.95	1006	193	0.012	298	830	0.090
80.8	0.50	514	193	0.048	397	599	0.070
78.4	0.51	519	185	0.11	509	1502	0.16
79.7	0.51	520	189	0.044	524	1530	0.16
81.0	0.51	521	184	0.036	503	1474	0.16
81.4	0.51	524	186	0.033	499	1386	0.15
80.2	0.51	520	183	0.086	532	1824	0.19
159.3	0.51	521	191	0.033	596	2318	0.23
160.0	0.51	522	191	0.11	622	2828	0.27
160.2	0.51	527	190	0.055	600	2353	0.23
160.0	0.51	524	192	0.037	527	1496	0.16
160.0	0.51	527	189	0.041	522	1501	0.16
159.3	0.51	523	187	0.029	532	1667	0.17

*Ice thickness was calculated using the measured geometric area and weight of the deposited water with a value of 0.63 g cm^{-3} for bulk density of vapor-deposited water ice.

$$\text{(R5c)}\quad HO_2NO_{2(g)} + H_2O_{(s)} \rightarrow H_2O_{2(s)} + HNO_{3(s)}$$

On the basis of gas phase thermodynamics data, however, (R5c) is estimated to be endothermic by approximately 5 kcal mol^{-1} [*DeMore et al.*, 1994]. Since the HNO_4 samples used in the current experiments can be in fact prepared by the aqueous phase equivalent of the reverse of (R5c) [*Kenley et al.*, 1981], it is unlikely that significant quantities of HNO_3 can result from (R5c). However, we recognize that the thermochemical equilibrium between HNO_4 and HNO_3 as established in the original synthetic HNO_4 sample was greatly altered by the subsequent purification procedures employed and by the deposition of excess quantities of H_2O in forming the ice substrate. Consequently, some HNO_3 production is to be expected following HNO_4 uptake, although the conversion rate should be relatively slow at the lower temperatures. The thermodynamic consequences of HNO_3 and HNO_4 solvation and/or hydration may also serve to favor HNO_3 formation.

In order to investigate the nature of the condensed phase species, we conducted several programmed heatings of prepared substrates. Preparation of the substrates typically involved subjecting ice-coated and uncoated walls to 30 min of HNO_4 gas flow prior to the heating procedure. The substrates were heated for 30 min at a constant heating rate of approximately 3 K min^{-1}.

The only species observed to desorb from the substrates were HNO_4, HNO_3, H_2O_2, and H_2O, as deduced from their characteristic mass spectral fragmentation patterns. Temperature profiles for some of the relevant mass peaks are shown in Figure 5. In the case of Figure 5a, flowing HNO_4 gas through the cold Pyrex surface leads to observation of a very thin, slightly opaque frozen solid layer on the surface, and during the heating process, some transparent, presumably liquid, spots on the layer were observed. Desorption of HNO_4 from

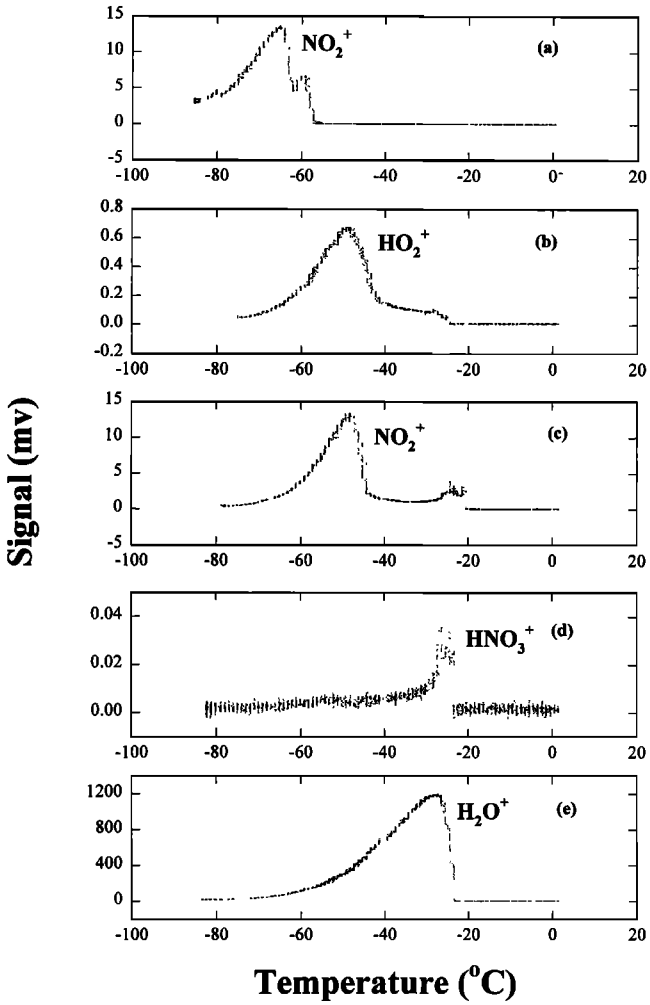

Figure 5. Signal intensity of different species as function of temperature after $\sim 10^{19}$ HNO_4 molecules were adsorbed on cold Pyrex and ice surfaces. (a) Desorption of HNO_4 detected as NO_2^+ from cold Pyrex surface, (b) desorption of HNO_4 detected as HO_2^+ from ice surface, (c) desorption of HNO_4 detected as NO_2^+ from ice surface, (d) desorption of HNO_3 detected as HNO_3^+ from ice surface, and (e) desorption of water ice detected as H_2O^+ from the coated ice film. About 1 g of H_2O was deposited in each experiment shown in Figures 5b–5e to make the ice films with thicknesses of about 160 μm. The heating rate for the desorption of product mixture was ~ 3 K min^{-1}.

"uncoated" glass reactor walls began at temperatures slightly above 193 K and peaked at 208 K. In sharp contrast, desorption of HNO_4 from ice-coated reactor walls (Figures 5b and 5c) occurred at significantly higher temperatures, starting at 210 K and reaching a maximum at 225 K; no transparent spots were observed during the warming of the solid. For the latter case the desorption temperature was independent of the ice film thickness. Since both cases actually involved HNO_4 and H_2O, albeit with vastly differing amounts of H_2O, the shift in the desorption temperatures between the two cases signals a significant change in the nature of the interaction between HNO_4 and the H_2O ice surfaces.

HNO_3 and H_2O desorbed from ice-coated reactor walls (Figures 5d and 5e) at roughly the same temperature (~ 246 K). Only small quantities of nitric acid were observed; comparison of integrated signal profiles indicates that the amounts of HNO_3 desorbed from the ice were less than 9% those of HNO_4. The likely origins of the observed HNO_3 were as impurities in the HNO_4 samples. In order to verify this hypothesis, we performed a temperature programmed desorption on two identically prepared HNO_4/H_2O ice substrates. One of the substrates was heated immediately following preparation, while the other was allowed to stand for about 3 hours at 193 K. No increase in the amount of desorbed HNO_3 was observed ($\pm 20\%$) in the second sample relative to the first. On the basis of this result we conclude that no appreciable heterogeneous reaction occurs between HNO_4 and H_2O ice which produces HNO_3. An upper limit of $<1\%$ was placed on the amount of HNO_3 produced by reaction of HNO_4 with H_2O ice over the timescale of the uptake.

Discussion

The results of the present study demonstrate that HNO_4 is rapidly adsorbed on H_2O ice surfaces at ~ 190 K. The measured uptake coefficient of 0.15 ± 0.10 is quite similar to that of the related acid HNO_3 [*Leu*, 1988; *Davy and Somorjai*, 1971; *Hanson*, 1992]. Like nitric acid, peroxynitric acid uptake on H_2O ice results only in condensed phase species. However, whereas the formation of solid solutions and hydrates has been well characterized in the HNO_3 case, phase relationships have not been explored for the HNO_4/H_2O system. In the present study we have probed only a small region of the phase equilibria. In particular, vapor phase conditions during HNO_4/H_2O deposition were nearly identical for the coated and uncoated reactor trials (i.e., $P(H_2O)/P(HNO_4) \approx 5$), and we expect that the same crystalline HNO_4 hydrate or amorphous solution, albeit unidentified, was formed initially in both cases, assuming that bulk diffusion of HNO_4 into the ice film was slow. Thus coexistence of this hydrate or amorphous solution with pure H_2O ice was the likely result of the ice-coated reactor trials and was also a possible outcome of the uncoated reactor trials.

The likely formation of three phases (hydrate/ice/vapor) in the coated reactor (i.e., excess H_2O) case constrains the system to only one degree of freedom. As a result the vapor pressures of HNO_4 and H_2O are fixed for any given temperature. Upon substrate warming the vapor pressures increase along the ice-hydrate solidus until the liquid/hydrate/ice eutectic point is reached. Further warming results in a phase change to the liquid/ice system. The absence of observable liquid formation in the coated reactor desorption trials, as would be evidenced by film transparency, indicates that the hydrate evaporation dominates over its melting process.

The observed ordering of evaporation and melting events in the coated reactor case can be related to the steady state (as opposed to static) nature of the experiments. Since the flow tube was subject to continuous vacuum pumping during the warming phase of the programmed desorption experiments, vapor phase species were removed from the reactor along with the carrier gas. Accordingly, the temperature dependent behaviors of observed gas phase species were governed both by the equilibrium vapor pressure over the substrates and the amounts of solid remaining in the flow tube. In a typical programmed desorption experiment, approximately 10^{19} molecules of HNO_4 were deposited on the substrate. The removal time of the HNO_4 depended on the equilibrium pressure; it was 10 min for HNO_4 pressure of 0.1 mtorr and only 1 min for pressures reaching 1 mtorr. On the basis of the observations we

conclude that the eutectic point corresponds to HNO_4 pressures of the order of 0.1 mtorr and the amount of initially deposited HNO_4 is insufficient to allow for the occurrence of the liquid phase change. By analogy with the nitric acid trihydrate (NAT)/ice system and on the basis of the lack of liquid formation upon heating the HNO_4 hydrate/ice system, we estimate that the hydrate/ice/liquid eutectic temperature could be located a few degrees higher than the temperature corresponding to the observed maximum HNO_4 vapor concentration (225 K).

The same reasoning applies to the HNO_3 observed desorption behavior. Given the gas phase conditions established during film deposition, we expected the impurity HNO_3 to form NAT on the ice surface. According to the HNO_3/H_2O phase diagram [*Hanson*, 1990], vapor pressures of HNO_3 in equilibrium with NAT/water ice range between 3×10^{-9} torr at 190 K and 2×10^{-5} torr at 230 K (eutectic temperature). On account of the relatively small equilibrium HNO_3 vapor pressure it did not require a large amount of HNO_3 in solution to maintain gas/condensed phase equilibrium conditions during the substrate warming. The amount of impurity HNO_3 deposited on the substrate ($\approx 10^{18}$ molecules), as determined from the integrated desorption signal (Figure 5d), was sufficient to allow the system to nearly reach the eutectic point and allowed us to see liquid formation in the reactor before all of the HNO_3-containing phases evaporated.

To further illustrate the behavior of HNO_3, we performed an additional programmed desorption experiment on ice substrate (160 μm thick) doped with approximately 4×10^{19} molecules of HNO_3. The result of the trial is showed in Figure 6. The absence of HNO_4 in the trial allowed us to monitor HNO_3 with higher sensitivity using the NO_2^+ fragment rather than the parent peak. The observed desorption behavior clearly supports the hypothesized initial formation of a NAT/ice solid. In particular, two HNO_3 desorption peaks are apparent at 228 K and 246 K, corresponding to eutectic and melting temperatures for NAT/ice/liquid and ice/liquid systems, respectively. On the basis of this information we conclude that an upper limit of ~20% of the 228 K peak observed in the PNA experiments could be due to HNO_3.

Vapor pressures of HNO_4 in the uncoated reactor case were significantly higher, for a given temperature, than those in the coated reactor. Moreover, the film evaporated at a significantly lower temperature (208 K) than the predominately ice-containing film. These observations suggest that for the uncoated reactor case the initially deposited hydrate/ice mixture rapidly became a pure hydrate after evaporation of the small amount of ice. By analogy with HNO_3 the equilibrium HNO_4 vapor pressure above the hydrate is presumably greater than that above a hydrate/ice mixture. As an example of this phenomena, *Koehler et al.* [1992] observed the evaporation of HNO_3 from pure NAT at a temperature 10 K below the ice/NAT/liquid eutectic temperature observed by us.

The HNO_4 hydrate properties deduced from the above discussion carry important implications for denitrification of atmospheric air parcels. Present experimental data suggest that the vapor pressure over the HNO_4 hydrate in equilibrium with ice is $\geq 10^{-6}$ torr at 190 K (see Figures 5a–5c), which is at least 2 orders of magnitude greater than the typical ambient HNO_4 concentration ($\leq 10^{-8}$ torr). Thus significant formation of this particular HNO_4 hydrate in either cirrus or polar stratospheric clouds is unlikely simply because there is not enough HNO_4 in the atmosphere. However, the HNO_4 may still stick to and occupy surface sites on both cloud types. Surface areas approaching 10^{-7} cm^2 cm^{-3} have been observed during polar stratospheric and cirrus cloud events [*Hamill and McMaster*, 1984; *McCormick et al.*, 1985]. Assuming monolayer coverage (i.e., $\sim 5 \times 10^{14}$ molecule cm^{-2}), we calculate that a large fraction of the ambient HNO_4 could be sequestered on the cloud particles.

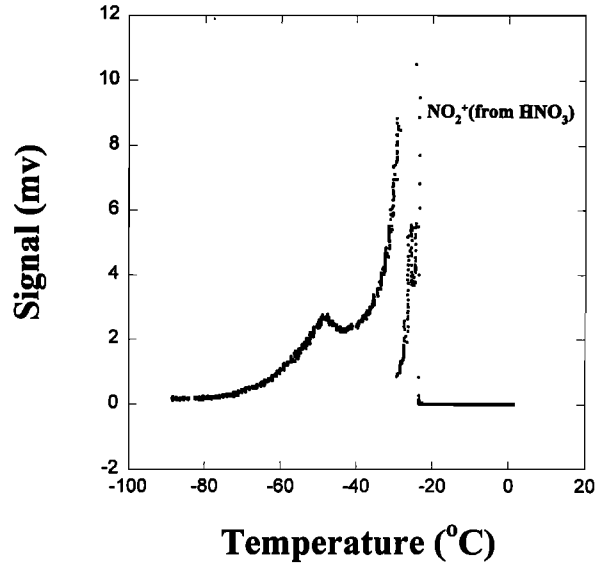

Figure 6. Nitric acid signal intensity (detected as NO_2^+) as function of temperature. The nitric acid was introduced on ice surface by passing the nitric acid vapor at 195 K through the reactor coated with ice film (160 μm thick). The heating rate was ~3 K min^{-1}.

The time required to fill the surface sites depends, of course, on the HNO_4 uptake coefficient. Although the coefficient measured in this study is strictly applicable only to HNO_4 concentrations well above ambient, we suspect that the coefficient depends only slightly on concentration, based on the observed invariance of the uptake coefficient for HNO_3 on ice at both high and low initial HNO_3 concentrations (10^{-4} and 10^{-7} torr, respectively [*Leu*, 1988; *Hanson*, 1992; M.-T. Leu, private communication, 1995]). Using the measured uptake coefficient of 0.15 for HNO_4 on ice, we estimate that HNO_4 removal by clouds will dominate over photolysis and reaction with OH and can occur on timescales of hours. This suggests that cloud scavenging of HNO_4 followed by large-scale gravitational settlement of Type II polar stratospheric clouds (PSCs) or rapid downward convection of cirrus may play a role in denitrification of particular air masses. This could lead to changes in the NO_x/NO_y ratio near the winter poles by removing NO_2.

A similar effect of HNO_4 heterogeneous chemistry on NO_y partitioning is not anticipated when one considers the global stratospheric aerosol background. A recent study found that the uptake coefficient of HNO_4 on liquid sulfuric acid surfaces decreased from 0.2 on 55 wt% H_2SO_4 to 0.06 on 70 wt % acid solution (R. Zhang et al., Heterogeneous chemistry of HO_2NO_2 on liquid sulfuric acid, submitted to *Journal of Physical Chemistry*, 1995). In addition, the background aerosol surface area is substantially less than observed during PSC events. Accordingly, the heterogeneous loss of HNO_4 due to the background sulfate aerosol should be less than 2% when HNO_4 monolayer coverage on aerosol surface is assumed. Hence it

appears that HNO_4 heterogeneous chemistry on cirrus and PSCs holds the only potential for impacting the modeling of the stratosphere and upper troposphere. The actual importance of the heterogeneous mechanism will depend on the degree of cloud evaporation, limitations on HNO_4 surface coverage due to saturation, and the possible existence of higher hydrates of HNO_4 with lower vapor pressures. Further investigations on the HNO_4/H_2O system are required to better address the atmospheric implications.

Acknowledgments. The research described in this paper was carried out at Jet Propulsion Laboratory, California Institute of Technology, under contract with the National Aeronautics and Space Administration. We thank G. T. Toon, M. R. Gunson, and R. J. Salawitch for providing their unpublished results, R. Zhang, M.-T. Leu, and R. J. Salawitch for helpful discussion on our results, and R. D. May for facility assistance in preparing HNO_4.

References

Anderson, J. G., J. J. Margitan, and F. Kaufman, Gas phase recombination of OH with NO and NO_2, *J. Chem. Phys.*, *60*, 3310–3317, 1974.

Brown, R. L., Tubular flow reactors with first-order kinetics, *J. Res. Natl. Bur. Stand. U.S.*, *83*, 1–8, 1978.

Considine, D. B., A. R. Douglass, and R. S. Stolarski, Heterogeneous conversion of N_2O_5 to HNO_3 on background stratospheric aerosols: Comparisons of model results with data, *Geophys. Res. Lett.*, *19*, 397–400, 1992.

Cox, R. A., The photolysis of gaseous nitrous acid, *J. Photochem.*, *3*, 175–188, 1974.

Davy, J. G., and G. A. Somorjai, Studies of the vaporation mechanism of ice single crystals, *J. Chem. Phys.*, *55*, 3624–3636, 1971.

DeMore, W. B., S. P. Sander, D. M. Golden, R. F. Hampson, M. J. Kurylo, C. J. Howard, A. R. Ravishankara, C. E. Kolb, and M. J. Molina, Chemical Kinetics and Photochemical Data for Use in Stratospheric Modeling, *JPL Publ. 94-26*, 1994.

Deshler, T., D. J. Hofmann, B. J. Johson, and W. R. Rozier, Balloonborne measurements of the Pinatubo aerosol size distribution and volatility at Laramie, Wyoming during the summer of 1991, *Geophys. Res. Lett.*, *19*, 199–202, 1992.

Fahey, D. W., K. K. Kelly, S. R. Kawa, A. F. Tuck, M. Loewenstein, K. R. Chan, and L. E. Heidt, Observations of denitrification and dehydration in the winter polar stratospheres, *Nature*, *344*, 321–324, 1990.

Graham, R. A., A. M. Winer, and J. N. Pitts Jr., Temperature dependence of the unimolecular decomposition of pernitric acid and its atmospheric implications, *Chem. Phys. Lett.*, *51*, 215–220, 1977.

Graham, R. A., A. M. Winer, and J. N. Pitts Jr., Pressure and temperature dependence of the unimolecular decomposition of HO_2NO_2, *J. Chem. Phys.*, *68*, 4505–4510, 1978a.

Graham, R. A., A. M. Winer, and J. N. Pitts Jr., Ultraviolet infrared absorption cross sections of gas-phase HO_2NO_2, *Geophys. Res. Lett.*, *5*, 909–911, 1978b.

Hamill, P., and L. R. McMaster (Eds.), Polar stratospheric clouds, their role in atmospheric processes, *NASA Conf. Publ.*, *2318*, 1–72, 1984.

Hanson, D. R., The vapor pressure of supercooled HNO_3/H_2O solutions, *Geophys. Res. Lett.*, *17*, 421–423, 1990.

Hanson, D. R., The uptake of HNO_3 onto ice, NAT, and frozen sulfuric acid, *Geophys. Res. Lett.*, *19*, 2063–2066, 1992.

Howard, C. J., Kinetics of the reaction of HO_2 with NO_2, *J. Chem. Phys.*, *67*, 5258–5263, 1977.

Howard, C. J., Kinetic measurements using flow tubes, *J. Phys. Chem.*, *83*, 3–9, 1979.

Hudson, R. D., and E. I. Reed, *The Stratosphere: Present and Future*, *NASA Ref. Publ.*, *1049*, 1979.

Kenley, R. A., P. L. Trevor, and B. Y. Yan, Preparation and thermal decomposition of pernitric acid ($HOONO_2$) in aqueous media, *J. Am. Chem. Soc.*, *103*, 2203–2206, 1981.

Keyser, L. F., and M.-T. Leu, Surface areas and porosities of ice used to simulate stratospheric clouds, *J. Colloid Interface Sci.*, *155*, 137–145, 1993.

Keyser, L. F., S. B. Moore, and M. T. Leu, Surface reaction and pore diffusion in flow-tube reactor, *J. Phys. Chem.*, *95*, 5496–5502, 1991.

Koehler, B. G., A. M. Middlebrook, and M. A. Tolbert, Characterization of model polar stratospheric cloud films using Fourier transform infrared spectroscopy and temperature programmed desorption, *J. Geophys. Res.*, *97*, 8065–8074, 1992.

Kondo, Y., W. A. Matthews, S. Solomon, M. Moike, M. Hayashi, K. Yamazaki, H. Nakajima, and K. Tsukui, Ground-based measurements of column amounts of NO_2 over Syowa Station, Antarctica, *J. Geophys. Res.*, *99*, 14,535–14,548, 1994.

Leu, M.-T., Laboratory studies of sticking coefficients and heterogeneous reactions important in the Antarctic stratosphere, *Geophys. Res. Lett.*, *15*, 17–20, 1988.

Logager, T., and K. Sehested, Formation and decay of peroxynitric acid: A pulse radiolysis study, *J. Phys. Chem.*, *97*, 10,047–10,052, 1993.

May, R. D., and R. R. Friedl, Integrated band intensities of HO_2NO_2 at 220 K, *J. Quant. Spectrosc. Radiat. Transfer*, *50*, 257–266, 1993.

McCormick, M. P., P. Hamill, and U. O. Farrukh, Characteristics of polar stratospheric clouds as observed by SAM II, SAGE, and Lidar, *J. Meteorol. Soc. Jpn.*, *63*, 267–276, 1985.

Molina, L. T., and M. J. Molina, UV absorption cross sections of HO_2NO_2 vapor, *J. Photochem.*, *15*, 97–108, 1981.

Molina, M. J., T.-L. Tso, L. T. Molina, and F. C.-Y. Wang, Antarctic stratospheric chemistry of chlorine nitrate, hydrogen chloride, and ice: Release of active chlorine, *Science*, *238*, 1253–1257, 1987.

Niki, H., P. D. Maker, C. M. Savage, and L. P. Breitenback, Fourier transform IR spectroscopic observation of pernitric acid formed via $HOO + NO_2 \rightarrow HOONO_2$, *Chem. Phys. Lett.*, *45*, 564–566, 1977.

Turco, R. P., R. C. Whitten, and O. B. Toon, Stratospheric aerosols: Observation and theory, *Rev. Geophys.*, *20*, 233–279, 1982.

Zhu, T., G. Yarwood, J. Chen, and H. Niki, Evidence for the heterogeneous formation of nitrous acid from peroxynitric acid in environmental chambers, *Environ. Sci. Technol.*, *27*, 982–983, 1993.

R. R. Friedl, S. B. Moore, and S. P. Sander, Jet Propulsion Laboratory, California Institute of Technology, Mail Stop 183-901, 4800 Oak Grove Drive, Pasadena, CA 91109.

Z. Li, Department of Atmospheric Sciences, University of Illinois at Urbana-Champaign, 220 Atmospheric Sciences Building, 105 Gregory Street, Urbana, IL 61801. (e-mail: zli@atmos.uiuc.edu)

(Received August 1, 1995; revised December 13, 1995; accepted December 13, 1995.)